

A comparison of hard X-ray photon indices and iron $K\alpha$ emission lines in X-ray luminous narrow- and broad-line Seyfert 1 galaxies

Xin-Lin Zhou

Key Laboratory of Optical Astronomy, National Astronomical Observatories, Chinese Academy of Sciences, Beijing 100012, China

Department of Physics and Tsinghua Center for Astrophysics, Tsinghua University, Beijing 100084, China

Shuang-Nan Zhang

Key Laboratory of Particle Astrophysics, Institute of High Energy Physics, Chinese Academy of Sciences, Beijing 100049, China

Physics Department, University of Alabama in Huntsville, Huntsville, AL 35899, USA

zhouxl@nao.cas.cn, zhangsn@ihep.ac.cn

ABSTRACT

We use publicly available XMM-Newton data to systematically compare the hard X-ray photon indices, $\Gamma_{2-10 \text{ keV}}$ and the iron $K\alpha$ emission lines of narrow-line (NL) and broad-line Seyfert 1 (BLS1) galaxies. We compile a flux-limited ($f_{2-10 \text{ keV}} \geq 1 \times 10^{-12} \text{ erg s}^{-1} \text{ cm}^{-2}$) sample including 114 radio-quiet objects, with the 2–10 keV luminosity ranging from 10^{41} to $10^{45} \text{ erg s}^{-1}$. Our main results are: 1) NLS1s and BLS1s show similar luminosity distributions; 2) The weighted mean of $\Gamma_{2-10 \text{ keV}}$ of NLS1s, BLS1s and the total sample is 2.04 ± 0.04 , 1.74 ± 0.02 , 1.84 ± 0.02 , respectively; a significant anti-correlation between $\Gamma_{2-10 \text{ keV}}$ and $\text{FWHM}H\beta$ suggests that $\Gamma_{2-10 \text{ keV}} > 2.0$ may be taken to indicate X-ray luminous NLS1 type; 3) The 6.4 keV narrow iron $K\alpha$ lines from NLS1s are generally weaker than that from BLS1s; this would indicate a smaller covering factor of the dusty tori in NLS1s, if the line emission originates from the inner boundary region of the dusty torus in an AGN; 4) all the broadened iron $K\alpha$ lines with intrinsic width $\sigma > 0.5 \text{ keV}$ correspond to $\text{FWHM}H\beta \leq 4000 \text{ km s}^{-1}$.

Subject headings: accretion, accretion disks - line: profiles - X-rays: galaxies - surveys

1. Introduction

It was found that a power-law component dominates the observed X-ray spectra of Seyfert 1 galaxies above 2 keV (Mushotzky et al. 1980). Other complex spectral features can be modeled by reprocessing of the hard power-law continuum in the circumnuclear cold matter (Pounds et al. 1990), with the mean photon index $\Gamma \sim 1.9 - 2.0$ (Nandra & Pounds 1994), where $f(E) \sim E^{-\Gamma}$. Therefore, the hard photon index, $\Gamma_{2-10 \text{ keV}}$, characterize the basic X-ray spectral shape of Seyfert galaxies, giving important clues to the emission mechanism and source properties.

Narrow-line Seyfert 1 (NLS1) galaxies (Osterbrock & Pogge 1985) are a subset of Seyfert 1 galaxies conventionally defined from their optical parameters (see Komossa 2008 and references therein). Many previous studies have suggested that NLS1 galaxies may have softer X-ray spectra than those of broad-line Seyfert 1 (BLS1) galaxies (Laor et al. 1994; Boller, Brandt & Fink 1996; Wang, Brinkmann & Bergeron 1996). There is an anti-correlation between $\Gamma_{2-10 \text{ keV}}$ and FWHM of the optical $H\beta$ lines found in Seyfert 1 galaxies (Brandt, Mathur & Elvis 1997). Therefore, NLS1 galaxies have been generally believed to show softer X-ray spectra, similar to the high/soft-state spectra from Galactic X-ray binaries (Pounds, Done & Osborne 1995; Zhou et al. 2007). However, recent studies suggested that the anti-correlation shows large scatter (Piconcelli et al. 2005) and some NLS1 galaxies selected from the Sloan Digital Sky Survey do not display softer X-ray spectra (Zhou et al. 2006).

Fluorescent iron $K\alpha$ lines are the most prominent reprocessed features in the X-ray spectra of Seyfert galaxies. *XMM-Newton* observations revealed that a narrow iron $K\alpha$ line (NIKAL) at 6.4 keV is almost ubiquitous, with a substantial fraction of objects showing broadened iron $K\alpha$ line (BIKAL) emission (Reeves et al. 2006; Nandra et al. 2007, N07). NIKAL was suggested to provide information of the geometry of the molecular torus, indicating changing AGN populations (Zhou & Wang 2005; Bianchi et al. 2007). BIKAL probes the strong gravity and spin of a black hole (e.g., Fabian et al. 2009; see the review by Reynolds & Nowak 2003 and Miller 2007). Note that the line profile seems to be very different in different sources. Studying the line profile as a function of source type is useful for future iron line surveys, since it is still unclear whether NLS1s are different from BLS1s in terms of iron $K\alpha$ emission.

Here we make a systematic comparison of $\Gamma_{2-10 \text{ keV}}$ and the iron $K\alpha$ emission lines of NLS1s and BLS1s based on *XMM-Newton* observations of X-ray luminous Seyfert 1 galaxies. Throughout this letter, we use the cosmological parameters of $h_0=70 \text{ km s}^{-1} \text{ Mpc}^{-1}$, $\Omega_m = 0.27$, $\Omega_\Lambda = 0.73$ (Komatsu et al. 2009).

2. Sample and data reduction

We compile a flux-limited ($f_{2-10 \text{ keV}} \geq 1 \times 10^{-12} \text{ erg s}^{-1} \text{ cm}^{-2}$) and radio-quiet Seyfert 1 sample from the *XMM-Newton* archive, as listed in Table 1; 86 out of these 114 AGNs are included in the CAIXA catalogue (Bianchi et al. 2009a). The redshift range of the present sample is $z < 0.37$, with only seven objects having $z > 0.2$. The sample includes most of well-studied Seyfert 1 galaxies.

The data have been reduced as homogeneously as possible. Only the EPIC PN (Strüder et al. 2001) data are used in our analysis. The SAS v7.0 software¹, with the corresponding calibration files, are used for the data reduction. The X-ray events corresponding to patterns 0–4 for the PN data are selected; hot or bad pixels are also removed. We extract the source spectra from a circle within $40''$ of the detected source position, with the background being taken from the circular source-free regions; the CCD chip gaps are all avoided. The presence of background flaring in the observation has been checked and removed using a Good Time Interval file. We also check the pile-ups in the data with the SAS task *epatplot*. The response files are generated with the SAS tools *rmfgen* and *arfgen*.

The spectral fittings are performed via a basic model expressed as $phabs * zphabs * zedge(powerlaw + Nzgauss)$ in XSPEC (Arnaud 1996) over the 2–10 keV band; however the 2–7 keV band is used for 1H0707-495 since there is a sharp drop around 7 keV found in this object (Boller et al. 2002). Errors are quoted at the 90% confidence level. For 108 out of 114 objects in Table 1, there exist published spectral fitting results (see online material). We add an additional Gaussian in our fits, if there was evidence for such a component in the published fits; we only add a single Gaussian to obtain line measurements in the remaining 6 AGNs. We note that we have not tested independently the significance of including this additional component. All the fittings include the absorption due to the line-of-sight Galactic column density (Dickey & Lockman 1990). The neutral reflection model (Magdziarz & Zdziarski 1995) is also tried for each spectrum. However, these fits generally do not improve significantly in the 2–10 keV band compared with the power-law fits. Thus we use the results returned from the basic model.

3. Results

Panel (a) in Figure 1 shows the distribution of 2–10 keV luminosity for the whole sample (thin solid line), compared with that of NLS1s (thick solid line) and that of BLS1s (dotted

¹<http://xmm.esac.esa.int/>

line). The luminosity of the NLS1s and BLS1s spans the same range from 10^{41} to 10^{45} erg s^{-1} ; this is natural since this sample is flux-limited.

Panel (b) in Figure 1 shows the distribution of $\Gamma_{2-10 \text{ keV}}$ for the whole sample, compared with that of NLS1s and that of BLS1s. The vertical dashed lines denote the weighted means of that of NLS1s, BLS1s and the total sample, which are 2.04 ± 0.04 , 1.74 ± 0.02 , 1.84 ± 0.02 , respectively. We perform the generalized Wilcoxon test constructed in ASURV² (Isobe et al. 1986) to determine the probability that NLS1s and BLS1s in this sample were drawn from the same parent population. We obtain the test statistic value of 7.3, indicating that the probability $< 0.01\%$. This robust and non-parametric test shows compelling evidence for the different photon indices between NLS1s and BLS1s in this sample.

Panel (c) in Figure 1 shows the distribution of equivalent width (EW) of 6.4 keV NIKAL for the whole sample, compared with that of NLS1s and that of BLS1s. The vertical dashed lines denote the weighted means of that of NLS1s, BLS1s and the total sample, which are 40 ± 5 , 125 ± 7 , 105 ± 7 eV, respectively. 34 out of these 114 AGNs have only upper limit data, with 20 out of 37 NLS1s and 14 out of 77 BLS1s, respectively; the values of EW are taken as half of the upper limits. It can be seen that NIKALs from NLS1s are systematically weaker than that from BLS1s. The generalized Wilcoxon test shows the statistical value of 4.0, giving a probability of $< 0.01\%$ that NLS1s and BLS1s were drawn from the same parent population.

Figure 2 shows $\Gamma_{2-10 \text{ keV}}$ against $\text{FWHM}H\beta$ for AGNs with available broad $H\beta$ measurements. The anti-correlation is significant, with the Spearman’s coefficient of -0.59 ; the Spearman’s probability associated with this coefficient is $< 0.01\%$. A linear regression by applying the parametric expectation-maximization algorithm gives,

$$\Gamma_{2-10 \text{ keV}} = (2.20 \pm 0.05) - (1.0 \pm 0.01) \left(\frac{\text{FWHM}H\beta}{10^4 \text{ km s}^{-1}} \right). \quad (1)$$

This suggests $\Gamma_{2-10 \text{ keV}} > 2.0$ for $\text{FWHM}H\beta < 2000 \text{ km s}^{-1}$ in this sample. We therefore choose to label the AGN with $\Gamma_{2-10 \text{ keV}} > 2.0$ as X-ray luminous NLS1 type. This criterion is useful for understanding the intermediate Seyfert galaxies (Sy 1.8 and 1.9) whose broad-line regions are lightly obscured, and for AGNs lacking the follow-up optical spectroscopies found in extragalactic surveys.

A flattening is also likely around $\text{FWHM}H\beta \sim 4000 \text{ km s}^{-1}$ in Figure 2. We give a separate fit for AGNs with $\text{FWHM}H\beta < 4000 \text{ km s}^{-1}$ (so-called Population A sources,

² <http://astrostatistics.psu.edu/statcodes/asurv>

Sulentic et al. 2008),

$$\Gamma_{2-10 \text{ keV}} = (2.45 \pm 0.07) - (2.0 \pm 0.02) \left(\frac{\text{FWHM}H\beta}{10^4 \text{ km s}^{-1}} \right). \quad (2)$$

4. Broadened iron $K\alpha$ lines

N07 performed an *XMM-Newton* survey of BIKAL based on 37 observations of 26 luminous Seyfert galaxies. Since data with high ratios of S/N in the hard X-ray band are required to characterize the line profiles in detail, they only selected the objects with at least 30 thousands net counts in their EPIC PN spectra in the 2 – 10 keV band. They derived the BIKAL parameters from a homogeneous spectral analysis after taking into account the NIKAL emission and the absorption due to a zone of ionized gas along the line of sight.

Here we re-analyse the results obtained in N07. Figure 3 plots the distribution of BIKAL EW of NLS1s, compared with that of BLS1s listed in N07. Most of BLS1s show weak BIKAL emission. Plausibly NLS1s show a more homogeneous distribution. However, the generalized Wilcoxon test shows the statistic value of 1.4, indicating a probability of 0.15 that NLS1s and BLS1s were taken from the same parent population. This makes it difficult to draw a firm conclusion. The intrinsic width (σ) of BIKAL denotes the velocity dispersion of the line emission region. We also study σ listed in N07 as a function of $\text{FWHM}H\beta$ in Figure 4. All the large values ($\sigma > 0.5 \text{ keV}$) correspond to $\text{FWHM}H\beta \leq 4000 \text{ km s}^{-1}$.

5. Discussion

A NLS1 galaxy is conventionally defined from its optical line width ($\text{FWHM}H\beta < 2000 \text{ km s}^{-1}$). Zhu et al. (2009) had shown that for optically selected AGNs, NLS1s and BLS1s have the same average accretion rate (L/L_{Edd}) (see Figure 17c in Zhu et al 2009); however, the black hole mass is significantly correlated with the broad emission line width (see Figure 17a in Zhu et al 2009). They arrived at this conclusion by modeling the broad emissions lines of the SDSS sample with a physically realistic two-component model. For the flux limited (i.e., X-ray luminous) AGN sample used here, the luminosity distribution of NLS1s is indistinguishable from that of BLS1s (see Figure 1a). Therefore, NLS1s must have on the average higher L/L_{Edd} than BLS1s in this X-ray flux limited sample, given that NLS1s contain less massive black holes. Consequently the X-ray luminous sample presented here is biased towards a higher L/L_{Edd} for the narrower $H\beta$, unlike a significant fraction of the local optical AGN population (Heckman et al. 2005). Thus the anti-correlation

between $\Gamma_{2-10 \text{ keV}}$ and $\text{FWHM}H\beta$ shown in Figure 2 must be due to the higher L/L_{Edd} for the narrower $\text{FWHM}H\beta$, in agreement with previous works on the correlation between $\Gamma_{2-10 \text{ keV}}$ and L/L_{Edd} (e.g., Wang et al. 2004). This is further supported by the mean L/L_{Edd} of ~ 1.1 for NLS1s and 0.16 for BLS1s, respectively, as calculated from the data in Bianchi et al (2009a; see Table 1). Vasudevan & Fabian (2007) found that the bolometric correction, $L_{\text{Bol}}/L_{2-10 \text{ keV}}$, depends on L/L_{Edd} , with a transitional region at $L/L_{\text{Edd}} \sim 0.1$; below which the bolometric correction is typically 15-25, and above which it is typically 40-70. Thus NLS1s, with the mean $L/L_{\text{Edd}} \sim 1$ in Table 1, have a higher bolometric correction, resulting in a smaller ratio of X-ray luminosity to bolometric luminosity than BLS1s. This also agrees with the conclusion of Bianchi et al. (2009b) that NLS1s are X-ray weaker, relative to BLS1s.

NIKAL are almost ubiquitous features in the present sample. The weighted mean width of NIKAL is $1350 \pm 250 \text{ km s}^{-1}$ for a small *Chandra* sample (Yaqoob & Padmanabhan 2004), more than a factor of 2 lower than the weighted mean width of $H\beta$ of $3200 \pm 60 \text{ km s}^{-1}$ (Nandra 2006). This provides compelling evidence that NIKAL is mainly emitted from the inner boundary region of the dusty torus in an AGN (Zhu et al. 2009). This agrees with previous suggestions that NIKAL unlikely originates from either the outer region of the accretion disk or the self-gravity-dominated disk (Zhou & Wang 2005) or the the broad-line region (Wu et al. 2009). In particular, the X-ray variability can not account for the observed NIKAL EW variation (Jiang et al. 2007). That means, NIKAL may give measures of the covering factor of the dusty torus, indicating the changing AGN populations (Zhou & Wang 2005; Zhu et al. 2009). The relatively weaker NIKAL EW in NLS1 can be explained in terms of models that the radiation pressure blows the cold dusty gas away from the central engine (Fabian et al. 2008), or the outflow scenario which can be related with the high L/L_{Edd} (Komossa et al. 2008). If this is true, some NLS1 galaxies may have geometrically-thin tori, as indicated by their weaker NIKAL emission. Conversely, the tori in some AGNs can be very geometrically-thick, as indicated by their very large NIKAL EW. NIKAL thus is very useful to identify this rare type of buried AGNs, which are difficult to detect so far (Ueda et al. 2008).

BIKAL is believed to be associated with the accretion disk, probing the strong gravity of a black hole (Fabian et al. 1989; Laor 1991). Recently, Brenneman & Reynolds (2006) developed a disk-line model in which the black hole spin is a free parameter. This makes it possible to constrain the space-time geometry close to distant black holes via X-ray spectroscopy. The results from N07 show that most of BLS1 galaxies show weak BIKAL emissions, with the EW less than 100 eV (Figure 3). This is in good agreement with the theoretical expectation of Ballantyne (2009). The mean EW and σ of BIKAL in NLS1s are larger than that of BLS1s, indicating a smaller inner disk radius, in agreement with the expectation of the evaporation

disk model, in which the inner radius of the disk is anti-correlated with L/L_{Edd} (Liu et al. 1999).

6. Conclusions

We present an X-ray luminous ($f_{2-10 \text{ keV}} \geq 1 \times 10^{-12} \text{ erg s}^{-1} \text{ cm}^{-2}$) Seyfert 1 sample including 114 radio-quiet objects, with the $2 - 10 \text{ keV}$ luminosity ranging from 10^{41} to $10^{45} \text{ erg s}^{-1}$. The NLS1s and BLS1s span the same luminosity range. The weighted mean of $\Gamma_{2-10 \text{ keV}}$ of NLS1s, BLS1s and the total sample are 2.04 ± 0.04 , 1.74 ± 0.02 , 1.84 ± 0.02 , respectively. The anti-correlation between $\Gamma_{2-10 \text{ keV}}$ and $\text{FWHM}H\beta$ is strong with a flattening at $\text{FWHM}H\beta \sim 4000 \text{ km s}^{-1}$. We propose that $\Gamma_{2-10 \text{ keV}} > 2.0$ may be taken to indicate X-ray luminous NLS1 type, reflecting the higher accretion rate, L/L_{Edd} in these objects.

The observed ratio between the average line width of NIKAL and that of $H\beta$ provides evidence that NIKAL mainly originates from the inner boundary region of the dusty torus in an AGN. The weighted means of the equivalent width (EW) of NIKAL of NLS1s, BLS1s and the total sample are 40 ± 5 , 125 ± 7 , $105 \pm 7 \text{ eV}$, respectively. Other than a few cases, NIKAL from NLS1s are generally weaker than that from BLS1s, indicating a smaller torus covering fraction in NLS1s. Some objects with an exceptionally larger EW, which may indicate a larger covering factor of the dusty torus, may represent a rare type of buried AGNs. Based on our re-analysis of the results in Nandra et al. (2007), plausibly the broadened iron $K\alpha$ lines from NLS1s show a more homogenous distribution than that from BLS1s. All AGNs with large intrinsic widths of iron $K\alpha$ lines ($\sigma > 0.5 \text{ keV}$) have $\text{FWHM}H\beta \leq 4000 \text{ km s}^{-1}$. This may give important clues to target selections for future iron line surveys.

We acknowledge an anonymous referee for many helpful comments to improve the manuscript. We thank useful discussions with Done, C., Li, T.-P., Schulze, N., Lu, Y., Soria, R., Wang, J.-M., Ward, M., Zhang, Y.-H. and Zhao, Y.-H. XLZ thanks the support from China postdoctoral science foundation; SNZ thanks the support from Directional Research Project of the CAS under project No. KJCX2-YW-T03, the National Natural Science Foundation of China under grant Nos. 10821061, 10733010, 10725313, and 973 Program of China under grant 2009CB824800.

REFERENCES

- Arnaud, K. A. 1996, Astronomical Data Analysis Software and Systems V, A.S.P. Conference Series, Vol. 101, 1996, George H. Jacoby and Jeannette Barnes, eds., p. 17
- Ballantyne, D. R. 2010, ApJ, 708, L1
- Bianchi, S., Guainazzi, M., Matt, G., Fonseca Bonilla, N., & Ponti, G. 2009a, A&A, 495, 421
- Bianchi, S., Guainazzi, M., Matt, G., Fonseca Bonilla, N., & Ponti, G. 2009b, A&A, 501, 915
- Bianchi, S., Guainazzi, M., Matt, G., & Fonseca B. N. 2007, A&A, 467, L19
- Boller, T., Brandt, W. N., & Fink, H. 1996, A&A, 305, 53
- Boller, T. et al. 2002, MNRAS, 329, L1
- Brandt, W. N., Mathur, S., & Elvis, M. 1997, MNRAS, 285, L25
- Brenneman, L. W., & Reynolds, C. S. 2006, ApJ, 652, 1028
- Dickey, J. M., & Lockman, F. J. 1990, ARA&A, 28, 215
- Fabian, A. C., Vasudevan, R. V., & Gandhi, P. 2008, MNRAS, 385, L43
- Fabian, A. C. et al. 2009, Nature, 459, 540
- Fabian, A. C., Rees, M. J., Stella, L., & White, N. E. 1989, MNRAS, 238, 729
- Greene, J. E., & Ho, L. C. 2005, ApJ, 630, 122
- Heckman, T. M., Ptak, A., Hornschemeier, A., & Kauffmann, G. 2005, ApJ, 634, 161
- Isobe, T., Feigelson, E. D., & Nelson, P. I. 1986, ApJ, 306, 490
- Komatsu, E. et al. 2009, ApJS, 180, 330
- Komossa, S. 2008, RMxAC, 32, 86
- Komossa, S., Xu, D., Zhou, H., Storchi-Bergmann, T., & Binette, L. 2008, ApJ, 680, 926
- Jiang, P., Wang, J. X., & Wang, T. G. 2006, ApJ, 644, 725
- Laor A., 1991, ApJ, 376, 90

- Laor, A., Fiore, F., Elvis, M., Wilkes, B. J., & McDowell, J. C. 1994, *ApJ*, 435, 611
- Liu, B. F., Yuan, W., Meyer, F., Meyer-Hofmeister, E. & Xie, G. Z. 1999, *ApJ*, 527, 17
- Magdziarz, P., & Zdziarski, A&A, 1995, *MNRAS*, 273, 837
- Miller, J. M. 2007, *ARA&A*, 45, 441
- Mushotzky, R. F., Marshall, F. E., Boldt, E. A., Holt, S. S., Serlemitsos, P. J. 1980, *ApJ*, 235, 377
- Nandra, K., & Pounds, K. 1994, *MNRAS*, 268, 405
- Nandra, K. 2006, *MNRAS*, 368, L62
- Nandra, K., O’Neill, P. M., George, I. M., & Reeves, J. N. 2007, *MNRAS*, 382, 194 (N07))
- Osterbrock, D. E. & Pogge, R. W. 1985, *ApJ*, 297, 166
- Piconcelli, E., Jimenez-Baile, E., Guainazzi, M., Schartel, N., Rodrouez-Pascual, P. M., & Santos-Lle, M. 2005, *A&A*, 432, 15
- Piconcelli, E. et al. 2006, *A&A*, 453, 839
- Pietsch, W., Bischoff, K., Boller, Th., Doebereiner, S., Kollatschny, W., & Zimmermann, H.-U. 1998, *A&A*, 333, 48
- Pounds, K. A., Nandra, K., Stewart, G. C., George, I. M., & Fabian, A. C. 1990, *Nature*, 344, 132
- Pounds, K. A., Done, C., & Osborne, J. P. 1995, *MNRAS*, 277, L5
- Reeves, J. N. et al. 2006, *AN*, 327, 1079
- Reynolds C. S., & Nowak M. A. 2003, *Phys. Rep.*, 377, 389
- Rodríguez-Ardila, A., Pastoriza, M. G., & Donzelli, C. J. 2000, *ApJS*, 126, 63
- Strüder L. et al., 2001, *A&A*, 365, L18
- Sulentic, J. W., Zamfir, S., Marziani, P., & Dultzin, D. The Nuclear Region, Host Galaxy and Environment of Active Galaxies (Eds. Erika Bentez, Irene Cruz-Gonzalez, & Yair Krongold) *Revista Mexicana de Astronomía y Astrofísica (Serie de Conferencias)* Vol. 32, pp. 51-58 (2008)

- Vasudevan, R. V., & Fabian, A. C. 2007, MNRAS, 381, 1235
- Ueda, Y. et al. 2007, ApJ, 664, L79
- Wang, T., Brinkmann, W., & Bergeron, J. 1996, A&A, 309, 81
- Wang, J. M., Watarai, K. Y., & Mineshige, S. 2004, ApJ, 607, 107
- Wu, J., Vanden Berk, D. E., Brandt, W. N., Schneider, D. P., Gibson, R. R., & Wu, J. F. 2009, ApJ, 2009, ApJ, 702, 767
- Yaqoob T., & Padmanabhan U., 2004, ApJ, 604, 63
- Zhou, H. Y., Wang, T. G., Yuan, W., Lu, H. L., Dong, X., Wang, J. X., & Lu, Y. J. 2006, ApJS, 166, 128
- Zhou, X. L., & Wang, J. M. 2005, ApJ, 618, L83
- Zhou, X. L., Yang, F., Lv, X. R., & Wang, J. M. 2007, AJ, 133, 432
- Zhu, L., Zhang, S. N., & Tang, S. 2009, ApJ, 700, 1173

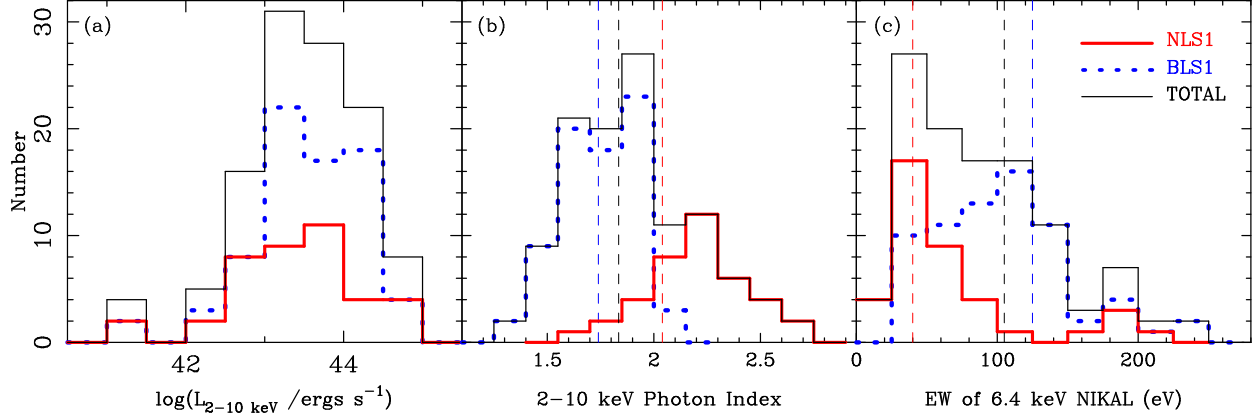


Fig. 1.— (a): The distribution of 2 – 10 keV luminosity for the whole sample (thin solid line), compared with that of NLS1s (thick solid line) and that of BLS1s (dotted line); (b): The distribution of the hard X-ray photon index for the whole sample, compared with that of NLS1s and that of BLS1s. The vertical dashed lines denote the weighted means of that of NLS1s, BLS1s and the total sample at 2.04 ± 0.04 , 1.74 ± 0.02 , 1.84 ± 0.02 , respectively; (c): The distribution of the equivalent width of the 6.4 keV narrow iron $K\alpha$ lines for the whole sample, compared with that of NLS1s and that of BLS1s. The vertical dashed lines denote the weighted means of that of NLS1s, BLS1s and the total sample at 40 ± 5 , 125 ± 7 , 105 ± 7 eV, respectively.

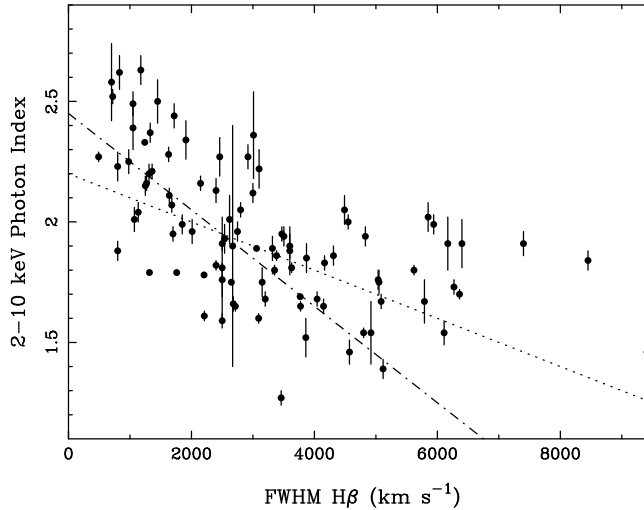


Fig. 2.— The hard X-ray photon index against FWHM of the broad $H\beta$ lines for AGNs with the $H\beta$ measurements available. The anti-correlation appears strong, but a flattening is likely around $\text{FWHM H}\beta \sim 4000 \text{ km s}^{-1}$. The dotted line denotes the best fit for the entire data given by Equation (1); the dotted-dashed line denotes the fit for AGNs with $\text{FWHM H}\beta < 4000 \text{ km s}^{-1}$ given by Equation (2).

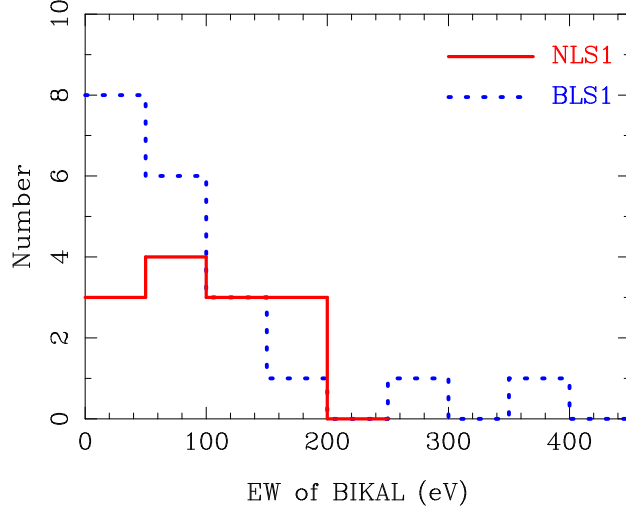


Fig. 3.— The distribution of the equivalent width of the broadened iron $K\alpha$ lines for NLS1s (thick solid line), compared with that of BLS1s (dotted line) in Nandra et al. (2007). Plausibly NLS1s show a more homogeneous distribution.

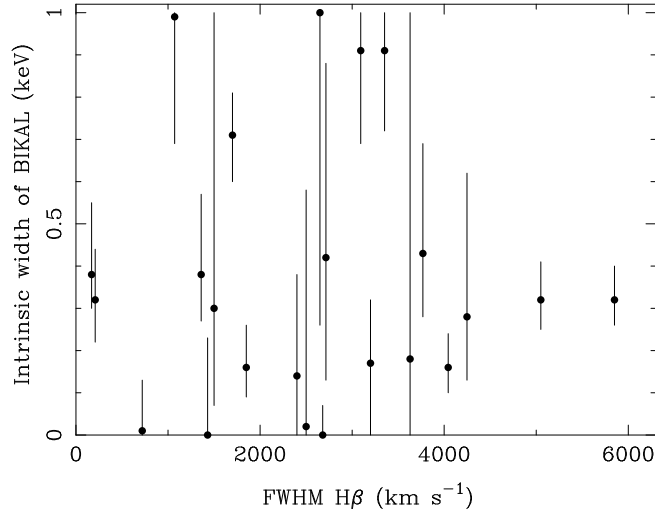


Fig. 4.— The intrinsic width of broadened iron $K\alpha$ lines as a function of $\text{FWHM H}\beta$ in Nandra et al. (2007). All the large width values (intrinsic width $\sigma > 0.5$ keV) correspond to $\text{FWHM H}\beta \leq 4000 \text{ km s}^{-1}$.

Table 1. *XMM-Newton* flux-limited sample of Seyfert 1 galaxies

Source (1)	Type (2)	$f_{2-10 \text{ keV}}$ (3)	$\Gamma_{2-10 \text{ keV}}$ (4)	EW(NIKAL) (5)	$L_{2-10 \text{ keV}}$ (6)	FWHM(H β) (7)	$\log(L/L_{\text{Edd}})$ (8)
Mrk 335	NLS1	13	2.28 ± 0.03	$\lesssim 54$	43.27	1629	0.05
1 Zw 1	NLS1	7.9	2.33 ± 0.01	34(4 – 64)	43.85	1240	0.12
PG 0052+251	BLS1	6.3	1.83 ± 0.03	$\lesssim 70$	44.61	4165	–0.83
Q 0056-363	BLS1	2.3	2.00 ± 0.03	153(115 – 195)	44.23	4550	–0.75
Ton S180	NLS1	4.5	2.25 ± 0.05	$\lesssim 64$	43.62	980	0.29
ESO 113-G10	NELG	2.7	1.91 ± 0.04	54(36 – 85)	42.58
Mrk 1152	BLS1	4.6	1.60 ± 0.05	141(100 – 180)	43.47
ESO 244-G17	BLS1	3.1	1.89 ± 0.05	142(128 – 156)	42.57	3317 ^a	...
Fairall 9	BLS1	18	1.73 ± 0.03	139(113 – 165)	43.97	6270	–1.72
NGC 526A	NELG	17	1.41 ± 0.06	78(51 – 105)	43.14
Mrk 359	NLS1	5.2	1.88 ± 0.04	205(139 – 274)	42.50	800	–0.60
Mrk 1014	NLS1	0.95	2.27 ± 0.08	$\lesssim 310$	43.85	2460	–0.11
Mrk 586	NLS1	1.7	2.39 ± 0.09	$\lesssim 103$	44.05	1050	0.53
Mrk 590	BLS1	4.7	1.66 ± 0.03	240(220 – 260)	42.86	2680	–0.16
Mrk 1044	NLS1	6.2	2.20 ± 0.04	186(125 – 247)	42.55	1310	0.02
ESO 416-G02	NELG	4.5	1.63 ± 0.05	$\lesssim 206$	43.58
ESO 198-G24	BLS1	3.9	1.91 ± 0.10	104(55 – 153)	43.27	6400	–1.36
RBS 416	NLS1	1.3	2.07 ± 0.03	$\lesssim 81$	43.20	1680	...
Mrk 609	NELG	1.4	1.64 ± 0.04	$\lesssim 299$	42.56
Fairall 1116	BLS1	5.3	1.86 ± 0.04	122(82 – 162)	43.63	4310	...
1H 0419-577	BLS1	7.7	1.27 ± 0.03	$\lesssim 82$	44.33	3460	–0.60
3C 120	BLS1	32	1.78 ± 0.01	54(30 – 78)	43.91	2205	–0.72
RBS 553	NELG	1.6	1.84 ± 0.04	$\lesssim 210$	43.30
H 0439-272	BLS1	5.6	1.91 ± 0.03	60(30 – 90)	43.98	2500	...
MCG-01-13-25	BLS1	7.8	1.76 ± 0.04	135(37 – 233)	42.85	5037 ^a	...
HE 0450-2958	NLS1	2.0	2.16 ± 0.03	$\lesssim 60$	44.61	1270	...
Ark 120	BLS1	38	2.02 ± 0.06	38(17 – 55)	43.95	5850	–0.99
MCG-02-14-09	BLS1	3.9	1.85 ± 0.06	165(78 – 255)	42.82	3871 ^a	...
MCG+8-11-11	BLS1	44	1.81 ± 0.02	88(72 – 104)	43.60	3630	–0.78
H0557-385	BLS1	42	1.89 ± 0.01	86(50 – 122)	44.03	3058 ^a	...
PKS 0558-504	NLS1	7.1	2.15 ± 0.04	$\lesssim 15$	44.55	1250	...
PMN J0623-6436	BLS1	3.6	1.96 ± 0.04	114(33 – 197)	44.19	2750 ^a	...
Mrk 6	BLS1	22	1.81 ± 0.21	95(71 – 109)	43.21	2500	...
1H 0707-495	NLS1	1.2	2.49 ± 0.05	59(33 – 98)	42.67	1050	–0.04
UGC 3973	BLS1	12	1.67 ± 0.03	178(160 – 196)	43.12	5086	–1.25
ESO 209-G12	BLS1	8.7	1.65 ± 0.02	104(60 – 151)	43.51	3774 ^a	...
PG 0804+761	BLS1	11	1.96 ± 0.05	100(40 – 170)	44.46	2012	–1.07
Fairall 1146	BLS1	9.5	1.57 ± 0.02	57(17 – 97)	43.32
PG 0844+349	BLS1	5.5	2.16 ± 0.03	$\lesssim 100$	43.74	2148	–0.77
MCG+04-22-42	BLS1	16	1.86 ± 0.02	115(62 – 171)	43.58
Mrk 110	NLS1	29	1.79 ± 0.01	49(39 – 59)	43.92	1760	–0.36
NGC 2992	NELG	85	1.53 ± 0.01	56(46 – 66)	42.97
MCG-5-23-16	NELG	74	1.90 ± 0.03	41(30-52)	43.02
PG 0947+396	BLS1	1.9	1.94 ± 0.04	120(60 – 180)	44.37	4830	–0.93
PG 0953+414	NLS1	3.2	2.12 ± 0.04	$\lesssim 50$	44.73	3000	–0.05

Table 1—Continued

Source (1)	Type (2)	$f_{2-10 \text{ keV}}$ (3)	$\Gamma_{2-10 \text{ keV}}$ (4)	EW(NIKAL) (5)	$L_{2-10 \text{ keV}}$ (6)	FWHM(H β) (7)	$\log(L/L_{\text{Edd}})$ (8)
HE 1029-1401	BLS1	11	1.91 ± 0.05	$\lesssim 102$	44.31	7400	−0.88
RE J1034+396	NLS1	0.9	2.58 ± 0.16	$\lesssim 171$	42.57	700	0.16
PG 1048+342	BLS1	1.4	1.90 ± 0.05	102(43 – 161)	44.04	3600	−0.85
Mrk 728	NELG	4.0	1.68 ± 0.05	145(100 – 190)	43.06
NGC 3516	BLS1	18	1.80 ± 0.02	196(174 – 218)	42.39	3353	−1.89
PG 1114+445	BLS1	2.6	1.46 ± 0.05	100(65 – 135)	44.16	4570	−0.86
PG 1115+407	NLS1	1.3	2.44 ± 0.05	$\lesssim 100$	43.93	1720	...
PG 1116+215	NLS1	3.5	2.27 ± 0.05	$\lesssim 80$	44.49	2920	−0.01
RBS 980	NELG	2.4	1.79 ± 0.05	145(135 – 155)	42.88
NGC 3783	BLS1	59	1.60 ± 0.02	116(103 – 129)	43.03	3093	−1.36
HE 1143-1810	BLS1	28	1.82 ± 0.02	53(39 – 65)	43.82	2400	...
NGC 4051	NLS1	28	2.01 ± 0.05	93(82 – 104)	41.39	1072	−1.5
PG 1202+281	BLS1	3.6	1.75 ± 0.05	$\lesssim 80$	44.43	5050	−0.45
NGC 4151	BLS1	83	1.65 ± 0.03	187(184 – 190)	42.22	4148	−1.39
PG 1211+143	NLS1	3.2	1.79 ± 0.01	40(10 – 60)	43.70	1317	−0.56
Mrk 766	NLS1	45	2.21 ± 0.03	41(20 – 61)	43.16	1360	−0.26
PG 1216+069	BLS1	1.4	1.67 ± 0.09	$\lesssim 70$	44.72	5790	−1.50
Mrk 205	BLS1	7.4	1.75 ± 0.06	60(35 – 85)	43.95	3150	−0.57
Ark 374	BLS1	3.2	1.94 ± 0.04	85(38 – 128)	43.49	3504	...
NGC 4579	NELG	3.9	1.78 ± 0.08	112(70 – 144)	41.11
NGC 4593	BLS1	65	1.69 ± 0.01	98(77 – 119)	43.07	3769	−0.79
Was 61	NLS1	4.9	2.11 ± 0.03	41(20 – 62)	43.33	1640	...
PG 1244+026	NLS1	2.6	2.62 ± 0.07	$\lesssim 146$	43.15	830	0.12
ESO 323-G77	BLS1	9.2	1.76 ± 0.07	111(79 – 144)	42.67	2500	...
PG 1307+085	BLS1	1.8	1.52 ± 0.08	$\lesssim 110$	44.08	3860	−1.18
NGC 5033	NELG	3.1	1.94 ± 0.03	109(59 – 169)	41.11
PG 1322+659	NLS1	1.3	2.22 ± 0.08	180(70 – 290)	44.02	3100	−0.24
MCG-6-30-15	NLS1	73	1.95 ± 0.03	52(42 – 62)	42.90	1700	−0.81
IRAS 13349+2438	NLS1	2.2	2.05 ± 0.03	$\lesssim 84$	43.81	2800	−0.58
NGC 5273	NELG	6.7	1.42 ± 0.09	233(168 – 296)	41.43
4U 1344-60	BLS1	49	1.54 ± 0.13	...	43.24	4920 ^a	...
IC 4329A	BLS1	160	1.80 ± 0.02	44(39 – 49)	43.96	5620	−0.83
Mrk 279	BLS1	16	1.86 ± 0.02	78(58 – 101)	43.50	3385	−0.81
PG 1352+183	BLS1	2.1	1.88 ± 0.10	150(70 – 230)	44.13	3600	−0.30
PG 1402+261	NLS1	1.9	2.34 ± 0.08	$\lesssim 100$	44.15	1910	0.26
NGC 5506	NLS1	85	1.99 ± 0.04	70(50 – 90)	42.83	1850	−0.38
PG 1411+442	BLS1	1.3	1.90 ± 0.50	225(135 – 315)	43.40	2670	−1.38
PG 1415+451	BLS1	1.2	2.01 ± 0.10	110(30 – 190)	43.60	2620	−0.77
NGC 5548	BLS1	38	1.68 ± 0.03	62(53 – 71)	43.39	4044	−1.63
PG 1416-129	BLS1	1.7	1.54 ± 0.05	60(30 – 90)	43.88	6110	−1.45
PG 1425+267	BLS1	1.9	1.46 ± 0.06	200(60 – 340)	44.94	9410	...
Mrk 1383	BLS1	6.8	1.99 ± 0.04	141(100 – 182)	44.10	5940	−1.07
PG 1427+480	BLS1	1.1	1.93 ± 0.06	90(40 – 140)	44.20	2540	−0.41
PG 1440+356	NLS1	3.7	2.50 ± 0.09	$\lesssim 80$	43.76	1450	0.09
PG 1448+273	NLS1	1.9	2.37 ± 0.04	74(15 – 134)	43.29	1330	0.43

Table 1—Continued

Source (1)	Type (2)	$f_{2-10 \text{ keV}}$ (3)	$\Gamma_{2-10 \text{ keV}}$ (4)	EW(NIKAL) (5)	$L_{2-10 \text{ keV}}$ (6)	FWHM(H β) (7)	$\log(L/L_{\text{Edd}})$ (8)
Mrk 841	BLS1	15	1.95 ± 0.03	125(75 – 148)	43.89	3470	–0.36
PKS 1514+00	NELG	1.7	1.70 ± 0.05	$\lesssim 81$	43.05
Mrk 290	BLS1	9.3	1.59 ± 0.03	43(12 – 74)	43.25	2500	...
Mrk 493	NLS1	3.6	2.23 ± 0.06	$\lesssim 105$	43.22	800	0.21
Mrk 876	BLS1	3.5	1.84 ± 0.04	96(37 – 155)	44.19	8450	–1.25
PG 1626+554	BLS1	3.1	2.05 ± 0.06	$\lesssim 160$	44.16	4490	–0.66
IRAS 17020+4544	NLS1	5.8	2.27 ± 0.02	$\lesssim 46$	43.70	490	0.51
PDS 456	NLS1	6.1	2.36 ± 0.18	$\lesssim 18$	44.77	3010	–0.11
IGR J17418-1212	BLS1	13	1.93 ± 0.04	54(27 – 80)	43.62
Mrk 509	BLS1	179	1.65 ± 0.02	85(28 – 142)	44.68	2715	–1.1
Mrk 896	NLS1	3.2	2.04 ± 0.04	180(93 – 267)	42.70	1135	0.17
Mrk 1513	NLS1	3.5	1.61 ± 0.02	64(29 – 101)	43.51	2210	...
CTS A08.12	BLS1	7.3	1.39 ± 0.04	100(80 – 120)	43.16	5118 ^a	...
NGC 7213	BLS1	34	1.68 ± 0.03	82(66 – 98)	42.27	3200	–1.79
Mrk 304	BLS1	6.4	1.91 ± 0.11	$\lesssim 115$	43.82	6170	–0.59
II Zw 177	NLS1	0.95	2.63 ± 0.06	$\lesssim 88$	43.22	1176	...
NGC 7314	NELG	54	2.19 ± 0.09	42(22–62)	42.28
ESO 602-G31	NELG	5.0	1.77 ± 0.04	140(138–152)	43.10
UGC 12138	NELG	7.9	1.87 ± 0.05	124(114–134)	43.05
Ark 564	NLS1	24	2.52 ± 0.03	40(20 – 60)	43.50	720	0.07
MR 2251-178	BLS1	29	1.54 ± 0.02	$\lesssim 74$	44.46	4800	...
NGC 7469	BLS1	26	1.75 ± 0.01	105(80 – 130)	43.17	2650	–0.49
Mrk 926	BLS1	30	1.70 ± 0.02	51(30 – 72)	44.17	6360	–1.78
AM 2354-304	NLS1	3.4	2.13 ± 0.05	$\lesssim 167$	42.85	2400	...

Note. — Col. (1): source name; Col. (2): source type. NELG: Narrow-emission-line galaxy, NLS1: Narrow line Seyfert 1 galaxy, BLS1: Broad line Seyfert 1 galaxy. NELGs are intermediate Seyfert galaxies whose broad line regions are lightly obscured. We take NELGs with $\Gamma_{2-10 \text{ keV}} > 2.0$ as NLS1s in our analysis; Col. (3): absorption-corrected 2–10 keV flux, in unit of $10^{-12} \text{ erg s}^{-1} \text{ cm}^{-2}$; Col. (4): 2–10 keV photon index; Col. (5): equivalent width (EW) of the 6.4 keV narrow iron K α line, in unit of eV. The intrinsic width is fixed at 10 eV for the EW measurements; Col. (6): log of the 2–10 keV luminosity, calculated from the 2–10 keV flux; Col. (7): FWHM of the broad H β line, in unit of km s^{-1} . Col. (8): Eddington ratio, calculated from the data available in Bianchi et al. (2009)a. ^a Object with the FWHMH β calculated from the FWHMH α using the relation $\text{FWMH}\beta = 1070 \times (\text{FWMH}\alpha/1000)^{1.03} \text{ km s}^{-1}$ given in Greene & Ho (2005). These objects have the FWHMH α measurements but lacking the FWHMH β measurements. FWHMH α of these objects are taken from Pietsch et al. (1998), Rodríguez-Ardila et al. (2000) and Piconcelli et al (2006), respectively.